LRP 669/00 May 2000

# Stationary Magnetic Entropy in Ohmic Tokamak Plasmas: Experimental Evidence From The TCV Device

E. Minardi & H. Weisen

submitted for publication in
Nuclear Fusion

ISSN 0458-5895

# STATIONARY MAGNETIC ENTROPY IN OHMIC TOKAMAK PLASMAS: EXPERIMENTAL EVIDENCE FROM THE TCV DEVICE

**Ettore Minardi**
Istituto di Fisica del Plasma "P. Caldirola"
Associazione EURATOM-ENEA-CNR
Milano, Italy

**Henri Weisen**
Centre de Recherches en Physiques des Plasmas
Association EURATOM-Confédération Suisse
Ecole Polytechnique Fédérale de Lausanne

***Abstract.*** The electron temperature, pressure and density profiles from a large variety of Ohmically heated plasmas in TCV (Tokamak à Configuration Variable, $B_T$<1.5T, $R_0$=0.88m, a<0.25m) are compared to theoretical predictions based on the principle of stationary magnetic entropy. These discharges include limited and diverted discharges with elongations in the range 1 to 2.54, triangularities between 0.5 and 0.72 and plasma currents in the range 0.1-1 MA. Over the entire range of quasi-stationary Ohmic conditions we observe that the sawtooth inversion radius and the electron temperature in the confinement region (outside the inversion radius), depend solely on the parameter $< j > /(q_0 j_0)$ where $< j >$ is the cross sectionally averaged current density. These observed sawtooth inversion radii and the electron temperature profiles are in excellent agreement with the predictions. The stiffness of the temperature profiles implies a correlation between density and pressure profiles, which is observed in the experiment. The observed electron pressure profiles are consistent with poloidal equilibria derived by combining the stationary magnetic entropy requirement with the Grad-Shafranov-Schlueter equation, although the actually observed range of pressure profiles is smaller than the theoretically accessible one.

**Table of contents**

### *1) Introduction*

Experimental observations and theoretical models supporting the idea that electron temperature and/or the pressure and/or current density in tokamaks preferentially assume certain privileged profile shapes have been reported for more than two decades [1-6]. Early observations in circular discharges have shown the edge safety factor $1/q_s$ to be the scaling factor for both the widths (or inverse peaking factor) for plasma profiles such as $<T_e>/T_{e0}$ and for the sawtooth inversion radius e.g. $< T_e > / T_{e0} \approx r_{inv} / s \approx 1/q_s$, where s is the minor radius. Recent observations in Ohmic plasmas in the TCV tokamak have shown that this behaviour is maintained for the full range of shaped plasmas that can be created in TCV [7-9]. The TCV tokamak (Tokamak à Configuration Variable, $B_T \leq 1.5$ T, $R_0 = 0.88$ m, $a \leq 0.25$ m) has an unprecedented flexibility for creating shaped plasmas [10]. These include elongations up to 2.58, triangularities ranging from –0.7 to 1, as well as plasmas with positive and negative "squareness", diverted and limited plasmas. A few examples of such plasmas are shown in fig.1. The edge safety factor $q_s$ ceases to be a meaningful scaling parameter in shaped plasmas. Instead of the above relation, valid only for circular discharges, we observe that

$$\frac{< T_e >}{T_{e0}} \approx \sqrt{\frac{A_{inv}}{A_p}} \approx \frac{< j >}{q_0 j_0}, \qquad (1.1)$$

as illustrated for the whole variety of discharges in fig.2 and fig.3. (The theoretically predicted lines in fig.3 will be explained later in the article). $< j >$ is the cross sectional average toroidal current density and $q_0 j_0 = (c/4\pi)(\kappa_0 + 1/\kappa_0) B_0 / R_0$, where $\kappa_0$, $B_0$ and $R_0$ are the elongation, toroidal magnetic field and major radius at the magnetic axis. $A_{inv}$ is the cross sectional area of the flux surface at which sawteeth invert and $A_p$ is the area of the discharge. Note that the general scaling parameter, $< j > /(q_0 j_0)$, is equal to $1/q_s$ in the large aspect ratio approximation for circular cross sections when corrections to the vacuum toroidal field are neglected.

The close relation between profile widths and sawtooth inversion radius can be understood from the "clipping" effect of the sawtooth crash. After a crash, plasma profiles are nearly flat inside the q=1 surface. Due to the rather low reheat power in Ohmic discharges only a moderate temperature increase is observed before the next sawtooth crash flattens the profiles again. As a result profiles remain fairly flat and their widths are closely correlated to the normalised inversion radius $\rho_{inv} = \sqrt{A_{inv} / A_p}$. As a result it was argued [7-9] that the observation of relations such as expressed by eq.(1.1) should not be regarded as supportive of

theories (often referred to as "profile consistency" theories) predicting similar relations without acknowledging the sawtooth phenomenon [3-5]. Sawteeth affect all Ohmic tokamak discharges operating in the usual range of edge safety factors (typically $q_{95}<10$). However the clipping effect cannot explain more subtle features in the confinement zone (outside de q=1 surface), which in TCV are also observed to scale with $< j > /(q_0 j_0)$. For high values of this scaling parameter, pressure and temperature profiles are close to trapezoidal outside the inversion radius, whereas they become increasingly concave as $< j > /(q_0 j_0)$ is reduced.

The aim of this article is to show that the profiles observed experimentally in the confinement region of TCV plasmas are consistent with the privileged profiles predicted in the framework of the magnetic entropy concept, a quantity that measures the probability of macroscopic plasma configurations. The statistical foundations of this concept, developed in previous papers, are briefly outlined in section 2 for the convenience of the reader, the main purpose of this paper being the application to the tokamak.

The tokamak is considered as an open system in interaction with the Ohmic transformer. In an open system the entropy is not required to be at a maximum, but it can be constant in time when the dissipative processes are counterbalanced by external sources. The theory does not require any explicit mention of the nature and dynamics of these dissipative processes. We note however that tokamak plasmas are host to a wealth of such processes in the form of microinstabilities, such as drift modes and micro-tearing modes, which are believed to be at the origin of anomalous transport. We consider a situation where the tokamak equilibrium in the confinement region (where the safety factor $q > 1$) is associated with a magnetic entropy that is constant in time. Such thermodynamic considerations are only applied to the confinement region where plasma parameters are relatively stationary and not to the core region, which does not reach a stationary state between consecutive sawtooth crashes.

The stationary entropy requirement implies strict conditions on the form of the current density profile in the confinement region, when boundary conditions are added, such as the position of the $q = 1$ surface. The position of, and current density at, the $q = 1$ surface are determined by the theoretical model for any given central safety factor $q_0$ consistent with experimental observations in sawtoothing tokamak discharges (typically $0.8 < q_0 < 1$).

Although the theory is derived for circular cross sections, the scaling factor $< j > /(q_0 j_0)$ introduced in [7-9] allows predictions to be extended to shaped cross sections. The theory establishes a relation between the $q = 1$ radius $r_{q=1}$, the axial safety factor $q_0$ and

the edge safety factor $q_s$, and predicts a rigid current profile for any given pair of parameter values ($r_{q=1}$, $q_0$) or ($q_s$, $q_0$). The experimental data for the sawtooth inversion radius, presented later in the paper, are in good agreement with the predicted $q=1$ radius. The experimental electron temperature profiles can be related to the predicted current density profiles using Ohm's law. They are also consistent with theoretical expectations and do indeed show the signatures expected from rigid current density profiles.

The compatibility of the requirement with the plasma force balance described by the Grad-Shafranov-Schlueter (G-S-S) equation involves significant restrictions on the form of the pressure profiles as compared to equilibria based on the G-S-S equation alone. Pressure profiles corresponding to a minimum of the plasma energy in the confinement zone at constant magnetic entropy and constant plasma current are predicted to be concave ($\nabla^2 p \geq 0$) in the confinement zone.

The sawtooth phenomenon is introduced in an adhoc fashion by assuming that pressure profiles be flat inside the $q = 1$ surface. This is fair assumption in the case of the sawtoothing Ohmic discharges discussed here, where the core region of the plasma is regularly flattened by sawtooth crashes and experiences only moderate reheating during the sawtooth ramp phases. The functional form of the pressure profile in the confinement region is completely determined once the quantity $< p > / \hat{p}$ is known, where $< p >$ is the volume average of the pressure (related to the total plasma energy content) and $\hat{p}$ is the pressure at the q=1 surface. The theory provides limitations on the values of $< p > / \hat{p}$ that are consistent with the observations, but provides no prediction of its behavior as function of the parameter $< j > / j_0 q_0$, such as is observed experimentally. The range of observed pressure profiles remains a small subset of the one allowed by this theory, suggesting that additional physics elements will need to be introduced in future developments in order to account for all observations.

In section 2 the theoretical underpinnings of the concept of magnetic entropy are presented and the basic expressions for the entropy functional are given. In section 3 the requirement of stationary entropy is combined with suitable boundary conditions for modeling stationary, sawtoothing, Ohmic tokamak plasmas. The expressions for the resulting current profiles are presented together with the expressions relating $r_{q=1}$, $q_0$ and $q_s$ and the functional forms for the pressure profile that follow from the requirement of compatibility with the G-S-S equation. The derivation of these expressions, being of purely technical character, is

postponed to appendix A. In section 4 the theoretical predictions are compared with the experimental observations in the TCV device. The minimum plasma energy principle, which is used for an alternative derivation of the permissible forms of the pressure profile and implications of the results for the thermal conductivity, are presented in appendixes B and C respectively.

### *2) The conceptual basis of the magnetic entropy*

The magnetic entropy is a measure of the probability of coarse-grained current density configurations in a suitably constrained possibility space (or "information space") of the magnetic plasma equilibria. The procedure for the construction of this concept and the discussion of its theoretical foundations have been developed previously [11,12, 13]. Here we limit ourselves to introducing the general concepts and to present the expressions that are used in the paper.

The plasma is considered in a macroscopic magnetic equilibrium, localized in a volume $\Omega$ in contact with an infinite background of fluctuating ions and electrons (neutral in the average) filling a volume $V >> \Omega$ . The background plays the formal role of a heat bath with which the plasma can exchange electric charges and energy.

The volume $V$ is divided into $N$ volume elements $\Delta V = V / N$ , which constitute the basic elements of the statistics. The assembly of $N$ volume elements can be arranged at random in the " information space", a $6N$-dimensional space$(\vec{j}_1,...\vec{j}_N;\vec{x}_1,...\vec{x}_N)$ whose coordinates are the position $\vec{x}_j$ in ordinary space (taking care that the positions cannot overlap) and the current density $\vec{j}_j$ to be ascribed to each one of the $N$ volume elements $\Delta V_j$. A point in the information space is representative of a particular current density distribution in the plasma and the information space is the site where all possible current density configurations can be represented and where the informations on the system can be introduced in the form of constraints on these configurations.

Here we adopt the Bayesian viewpoint where the constraints have a hypothetical meaning. [14,15]. Considering a large number of copies of the assembly of $N$ volume elements, an equilibrium ensemble in the sense of Gibbs is set up by assigning the probability distribution $p(\vec{j}_1,...\vec{j}_N;\vec{x}_1,...\vec{x}_N)$ for the assembly to occupy any given volume element $d\Gamma$ of the $6N$ -dimensional space $\Gamma(\vec{j}_1,...\vec{j}_N;\vec{x}_1,...\vec{x}_N)$ . The distribution $p$ is assigned by maximizing

the entropy $S = -\int_{\Gamma} p \ln p d\Gamma$ with respect to variations of $p$ under given constraints. The maximization of $S$ with respect to $p$ is a rule for assigning probabilities to the hypotheses expressed by the constraints [16,17].That is to say, one advances " testable constraints" that imply a determination (an assignment) of $p$ through the maximization of $S$ under the constraints. If the probability $p$ and the entropy $S$ calculated with these constraints prove to agree with the observations, then one infers the physical consistency of the constraints.

In our formulation the constraints imply essentially that the system fluctuates in information space around an assigned (a priory unspecified) macroscopic current density distribution with a given dispersion and with energy exchanged with the heat bath, such as to simulate the interaction of the system with the external world. The procedure leads to the following functional of the macroscopic current density distribution $\vec{j}(\vec{x})$ in $\Omega$ and of the related vector potential $\vec{A}(\vec{x})$ of the given macroscopic equilibrium [11]

$$S \propto -\int_{\Omega} j^2 dV + \frac{\mu^2}{4\pi}\int_{\Omega} \vec{j} \bullet \vec{A} dV \qquad (2.1)$$

where a positive factor and an inessential additive constant are omitted. The parameter $\mu$ is related to a Lagrange multiplier and can be considered as a free parameter, consistently with the mathematical formalism [11].

The current density may be determined by a further maximization of $S$ or only by assuming that $S$ is stationary, depending on the physical situation at hand. The former case is appropriate when the plasma is energetically isolated and one expects that the privileged magnetic equilibria are associated with a maximum $S$. This is the case of the (ideal) pinch, enclosed and isolated from the external world by a perfect conductive shell. One finds [18] that in this case the states of maximum entropy are the relaxed states of the Bessel function model [19] associated with those values of $\mu$ which correspond to stability. It is not, however, the case of the tokamak where the plasma interacts with the external world through the Ohmic transformer and the auxiliary heating.

A thermodynamic model of the tokamak, which takes into account the Ohmic interaction, can be formulated by including the time-dependent current of the primary of the transformer in the current density $\vec{j}$ entering $S$. One puts $\vec{j}(x) = \vec{j}_p(\vec{x}) + \vec{j}_S(t)$ , where $\vec{j}_p(\vec{x})$ is the stationary current density in the plasma volume and $\vec{j}_S(t)$ simulates the current in the

primary of the Ohmic transformer and is localized in a thin shell at the edge of the plasma column. By performing the time derivative of $S$ through $\vec{j}_S(t)$ and applying Maxwell's equations, the inductive toroidal electric field $\vec{E} = \vec{e}_\phi E$ (with $E = E_0 R_0 / R$ ) is introduced and the following expression for the time derivative of $S$ in an Ohmic tokamak is obtained (for a detailed exposition of this calculation see ref.[13].)

$$\frac{dS}{dt} \propto \int_{V_p} \left( \frac{\vec{E}}{\mu^2} \bullet \nabla^2 \vec{j}_p + \vec{E} \bullet \vec{j}_p \right) dV \qquad (2.2)$$

where $V_p$ is the plasma volume (excluding the shell) and an inessential factor has been omitted (henceforth the subscript $p$ of $\vec{j}_p$ will be dropped).

The comparison of (2.2) with the power balance equation leads to the identification of $dS/dt$ with the time derivative of the plasma energy [13] (apart from a proportionality factor that has the meaning of the inverse of a generalized temperature). The first term in the right hand side is identified with the heat diffusion (in a one-fluid approximation) while the last term is the work of the Ohmic electric field. Then the right hand side is proportional to the net heat that would be absorbed by the plasma in a reversible process and vanishes under stationary conditions. (Note that in the presence of auxiliary heating, a third term, representative of the heat deposition profile, appears at the right hand side in eq. (2.2)).

In the present paper we shall study those tokamak states which are associated with $dS/dt$ vanishing locally in the confinement region, namely the integral (2.2) is assumed to vanish when extended to any arbitrary toroidal ring $\Delta\Omega$ in a zone comprised between the values $q(s\lambda) = 1$ and $q_s = q(s)$ of the safety factor, where $r = r_{q=1} = s\lambda$ and $r = s$ are the inner and outer borders of the confinement region. Thus, in view of the arbitrariness of $\Delta\Omega$, the toroidal current density must satisfy the equation

$$\nabla^2 \vec{j} + \mu^2 \vec{j} = 0 \qquad (2.3)$$

The current and pressure distributions consistent with this equation are the object of the present investigations.

### *3) Tokamak Ohmic states with stationary magnetic entropy*

In this section we present the relations that will be the object of experimental scrutiny. They are a consequence of eq. (2.3) combined with the G-S-S equilibrium, as will be discussed in detail in Appendix A.

In cylindrical geometry the solution of (2.3) with the boundary conditions $j(s\lambda) = \hat{j}, j(s) = 0$ can be expressed in terms of Bessel functions

$$j(r) = \frac{\hat{j}}{D}\left(J_0(\mu s)Y_0(\mu r) - Y_0(\mu s)J_0(\mu r)\right) \tag{3.1}$$

where

$$D = J_0(\mu s)Y_0(\mu s\lambda) - Y_0(\mu s)J_0(\mu s\lambda) \tag{3.2}$$

Here and henceforth hats denote quantities on the $q=1$ surface. Using Ohm's law the expression (3.1) leads to a $T_e$ profile that will be compared with the experimental one. Furthermore the solution (3.1) entails the following relation for the experimentally relevant parameter $< j > / j_0 q_0$:

$$\frac{< j > B_0}{j_0 q_0 \hat{B}} = \lambda^2 - \frac{2q_0}{\mu s D}\left(\frac{2}{\pi \mu s} + \lambda\Lambda\right) \tag{3.3}$$

where

$$\Lambda = J_0(\mu s)Y_1(\lambda\mu s) - Y_0(\mu s)J_1(\lambda\mu s) \tag{3.4}$$

The equality (3.3) is basically a relationship between $< j > B_0 /(\hat{B} j_0 q_0)$ and the position $\lambda$ of the $q = 1$ surface. Indeed the numerical inspection of this relation shows that the other parameters $\left(B_{ext}/\hat{B}, q_0, j_0, \mu s\right)$ play only a secondary role for $0.8 < q_0 < 1$. In particular the dependence on $\mu s$ is negligible for $\mu s < 1$. Then, in view of this insensitivity, the $\lambda-$ dependence of $< j > B_0 /(\hat{B} j_0 q_0) \cong < j > /(j_0 q_0)$ is sufficiently robust to be the object of a comparison with experimental data.

A further subject of experimental investigation is the pressure profile of the G-S-S equilibrium that is compatible with a magnetic entropy that is stationary locally, as is derived in Appendix A

$$\frac{p}{\hat{p}} = \frac{\Psi}{\hat{\Psi}} + \frac{Y}{\hat{X}}(K-1) \tag{3.5}$$

Here $\Psi$ is a dimensionless poloidal flux related to the real flux $\psi$ by the equality $\Psi = \left(\mu^2 / 2\hat{B}\right)\psi$. The functions $X$ and $Y$ are defined as follows

$$X(\Psi) \equiv \int_0^{\Psi} d\Psi \ln x, Y(\Psi) \equiv \hat{X}\frac{\Psi}{\hat{\Psi}} - X(\Psi) \tag{3.6}$$

where $x = r/s$ is the normalized radius. It will be shown in Appendix A that the parameter $K$ depends on the global poloidal configuration through $< j > / j_0 q_0$ and $< p > / \hat{p}$, $< p >$ being the average of the pressure in the whole plasma volume including the sawteeth zone, where $p$ is taken as uniform. The theory then predicts that the pressure profile is completely determined once the two parameters above are known. However, the theory in its present form does not determine the numerical value of $< p > / \hat{p}$ and hence of $K$. It follows from eq. (3.5) that $K$ must be positive in order for $p$ to be positive. Moreover $K$ characterizes the curvature of the profile $p(\Psi)$

$$p''(\Psi) = \hat{p}(1-K)\frac{c\hat{B}}{\mu^2 R_0 \hat{X} I(\Psi)} \tag{3.7}$$

where $I(\Psi)$ is the current flowing inside $\Psi$.

An alternative derivation of the pressure profile (eq. 3.5) is given in Appendix B where this equation is derived from the condition that the plasma energy be an extremum for a constant magnetic entropy and a constant total current. The extremum is a minimum if $K < 1$. This implies that the pressure profile is concave, according to eq.(3.7). However the numerical value of $K$ remains undetermined by this theory.

### *4) Privileged equilibria in the experiment*

We are now in a position to compare theoretical predictions to experimental observations. The experimental data are a subset of the TCV confinement and profile database CONFDB and span a wide range of Ohmic L-mode plasma conditions. The dataset is identical with the one presented in ref. [7-9] and spans the following parameter range:

| | |
|---|---|
| Elongation at LCFS: | $1 \le \kappa_s \le 2.54$ |
| Triangularity at LCFS: | $-0.5 \le \delta_s \le 0.72$ |
| Squareness at LCFS: | $-0.1 \le \zeta_s \le 0.3$ |
| Safety factor at 95% flux: | $2 < q_{95} < 7$ |
| Dimensionless average current density: | $0.4 \le 4\pi R_0 < j > /(cB_0) \le 1.8$ |
| Current density width: | $0.17 \le < j > /(q_0 j_0) \le 0.63$ |
| Plasma current: | $100\ \mathrm{kA} \le I_p \le 1.02\ \mathrm{MA}$ |
| Average electron density: | $1.2\times10^{19}\ \mathrm{m}^{-3} \le \bar{n}_e \le 1.2\times10^{20}\ \mathrm{m}^{-3}$ |
| Central electron temperature: | $0.5 \le T_e(0) \le 1.1\ \mathrm{keV}$ |
| Poloidal beta: | $0.05 \le \beta_p \le 0.85$ |
| Collisionality at 75% flux: | $0.1 \le \nu^*_{75} \le 10$ |

The confinement properties of these plasmas have been presented in ref. [20]. Symbols used in fig.2, fig.3 and fig.7 are identical to those used in ref. [7-9,20] to distinguish categories of plasma elongation. Since the plasma properties discussed in this article are independent of plasma shape when expressed using the appropriate variables, shape distinction is not maintained for most figures. It should however be kept in mind that fig.2, fig.6, fig.7, fig.11, fig.12 and fig.13 represent exactly the same dataset. Fig.3 is from a smaller subset of the same data because X-ray tomography for the determination of sawtooth inversion radii [21,22] was not available for all samples.

*4-1 Location of the $q=1$ surface*

In fig.3 the relation (3.3), for $q_0$ in the range 0.8-1, is compared with the experimental data. Although there is no such measurement available on TCV, this range of axial safety factors is consistent with the experimental values obtained from different devices [23-26]. The parameter μs was chosen to be equal to 0.1. As noted in section 3, for μs<1 the predictions are indistinguishable in practice and this parameter can be taken to be arbitrarily small. As an important consequence, the parameter μ does not introduce a degree of freedom.

It is more difficult, from a point of view of principles, to deal with corrections to the equilibrium field when scaling the predictions from circular to shaped. Theory suggests that the scaling factor should be $< j > B_0 /(j_0 q_0 \hat{B})$, which is indeed very close to the semi-empirical scaling factor $< j > /(j_0 q_0)$ mentioned in the introduction. The vacuum field correction in the database is well approximated by

$$B_0 / \hat{B} \approx 1 + 0.032(1-\beta_p) < j >^{*2} \qquad (4.1)$$

where $< j >^{*} = (4\pi / c) R_0 < j > / B_{ext}$ is the dimensionless average current density of the discharge [7-9]. For tokamak discharges with circular cross sections we have $< j >^{*} /2 = (B_0 / B_{ext}) < j > /(j_0 q_0) \cong < j > /(j_0 q_0)$.

The vacuum field correction $B_0 / \hat{B}$ is 1.1% for circular plasmas with the highest value of $< j > / j_0 q_0$, although it is as high as 7-9% in the most elongated cases ($\kappa_a$>2.2) which also have extreme average current densities and strong paramagnetism. For the comparisons to follow, each (shaped) discharge in the database is compared to a circular theoretical model having the same value of $< j > /(j_0 q_0)$ and the same value of $\beta_p$. The vacuum field corrections for the circular model plasmas calculated using eq.(4.1) with the experimental values of $\beta_p$ and $< j > /(j_0 q_0)$ are effectively negligible and introduce no significant trends in the data.

Although a value of $q_0 \cong 0.8$ appears to fit the experimental data points in fig.3 best, this should not be taken as an indication of the "actual" value, since inversion radii need not coincide exactly with the q=1 surface. For the remainder of the paper we'll choose $q_0 = 0.9$ as a typical value for the central safety factor. Different choices of $q_0$ in the range 0.8-1 do not affect the comparison significantly. From fig.3 we also see that theory predicts a vanishing sawtooth inversion radius for $< j > /(q_0 j_0) < 0.1$, which is consistent with experiment. We

conclude that the poloidal magnetic configuration is essentially determined by $\lambda$ (or alternatively, by $< j > B_0 /(j_0 q_0 \hat{B})$).

*4-2 Dependence of the pressure profile on the current density profile*

Fig.4 shows the theoretical profiles of the current density and of the corresponding pressure for different values of the convexity parameter $K$ in the case of a poloidal magnetic equilibrium specified by $\lambda = 0.4, q_0 = 0.9$.

In fig.5 the normalised experimental pressure profile for a high and a low value of $< j > / q_0 j_0$ are compared with the theoretical profiles calculated for values of $K$ chosen to provide a good match of experimental and theoretical profiles in the confinement zone. This implies low values of K for low values of $< j > / q_0 j_0$ and values in the range 0.4-0.8 for the highest values of $< j > / q_0 j_0$.

The above definition of $K$ assumes that $p$ is flat in the sawteeth zone, as seen in eq.(A.18). Since even Ohmic plasmas experience a finite, albeit modest amount of reheat between sawtooth crashes, comparisons with theory need to take this into account by disregarding the pressure peaking inside the sawteeth zone. To this effect we define a "clipped" experimental pressure profile as follows

$$\overline{p} = \min(p, \hat{p})$$

where $\hat{p}$ is the pressure at the q=1 surface. Since the q=1 surface essentially coincides with the sawtooth inversion radius (fig.3), $\hat{p}$ is, unlike $p_0$, well defined independently of the time at which the measurement is taken during the sawtooth cycle. The experimental clipped electron pressure profile width $< \overline{p}_e > / \hat{p}_e$ can then be compared to the theoretical width $< p > / \hat{p}$.

In fig.6 the experimental widths of both the electron pressure profile $< p_e > / p_{e0}$ (triangles) and the clipped electron pressure profile $< \overline{p}_e > / \hat{p}_e$ (diamonds) are plotted versus $< j > / q_0 j_0$ assuming $q_0 = 0.9$. The former exhibit considerable scatter because the measurements were taken at predefined pulsing times of the Thomson scattering system, which are random with respect to the sawtooth cycle. The latter, on the contrary, are

very well correlated with $< j > / q_0 j_0$. We observe a linear relationship such that $< \overline{p}_e > / \hat{p}_e \cong \gamma < j > /(q_0 j_0)$. The value obtained for $\gamma$ depends weakly on the assumed value of $q_0$: $\gamma \cong q_0^{-1/2}$. (Note that in the figures quantities on the q=1 surface are referred to by the subscript "1", e.g. $p_{e1}$ for electron pressure, whereas in the text the diacritical mark ^ is used.)

It will be shown in Appendix B that a pressure profile of the form given by eq.(3.5) can be derived from the condition that the plasma energy be an extremum for a fixed current and a fixed magnetic entropy of the poloidal equilibrium. The extremum is a minimum if $K < 1$. This implies that the pressure profiles are concave, in accordance with (3.7). Fig.4 shows examples of pressure profiles corresponding to the boundaries of the allowable values of $K$ (dash-dotted), an example of a 'forbidden' convex pressure profile (dotted) and a typical pressure profile (continuous line) such that $\gamma \cong 1$.

Using eq.(A.20), the experimentally measured widths $< \overline{p}_e > / \hat{p}_e$ in fig.6 can be associated with corresponding values of the convexity parameter $K$, shown in fig.7. With a few exceptions, attributable to experimental uncertainties, the experimental values do indeed lie in the interval $0 < K < 1$. It is immediately apparent that the values of $K$ are not arbitrarily distributed in the allowable interval, but are strongly correlated with $< j > / q_0 j_0$. Fig.8 shows for several values of $K$ how the theoretical ratio of the pressure peaking to the current profile peaking factor, $\gamma$, varies with $< j > / q_0 j_0$, assuming $q_0$=0.9. In this plot the experimental observations (not shown) would populate a narrow horizontal band around $\gamma = 1.04$.

### *4-3 Consistency with Ohm's law*

In a stationary Ohmic tokamak discharge the current profile is related to the temperature, pressure and density profiles by Ohm's law:

$$j = \sigma E + j_{boot}.$$

In its simplest form Ohm's law is given by the Spitzer conductivity ($\sigma_{Spit} \propto T_e^{3/2}$) and the bootstrap current, which is typically only a few percent in most Ohmic discharges, is neglected. If electron and ion profiles are assumed to be proportional to each other, Ohm's

law, together with the definition of pressure, $p = k_B \sum n_{e,i} T_{e,i}$ allows us to calculate the temperature and the density profiles for given current and pressure profile. This has been done in the example of fig.9, which shows these profiles for one of the discharges already presented in fig.5, together with experimental profiles. The theoretical current profile is fixed by the value of $< j > / q_0 j_0$, which is equal to 0.62 in this case. When only Spitzer conductivity is considered, the temperature profile in the confinement zone is simply given by $T_e / \hat{T}_e = \left(j / \hat{j}\right)^{2/3}$ and the density profile is obtained from $n_e / \hat{n}_e = \frac{p_e / \hat{p}_e}{\left(j / \hat{j}\right)^{2/3}}$.

These profiles correspond to the dashed lines in fig.9. Theoretical profiles consistent with the neo-classical Ohm's law, shown as continuous lines, are obtained iteratively, starting from the Spitzer case and using measured absolute values of temperature, density and $Z_{eff}$. In practice the differences are so small that a single iteration beyond the Spitzer starting value is sufficient. For the neo-classical calculation the coefficients were taken from ref.[27].

As seen in fig.9, the temperature profile is barely influenced by the neo-classical effects introduced by pressures and collisionalities such as obtained in the experiment. One would therefore expect a high degree of 'profile stiffness' for the temperature profile, while pressure and density profiles would have more freedom. The widths of these profiles are expected to be closely correlated as shown in the theoretical predictions of fig.10 for three values of $\lambda$.

Such behaviour is indeed borne out in the experiment, as shown in fig.11 for the temperature profile. The measured electron temperature profile widths (diamonds) in the confinement zone, $< \overline{T}_e > / \hat{T}_e$ are closely related to $< j > / q_0 j_0$ and very close in absolute value to the prediction (dots) assuming a fixed value $q_0 = 0.9$. These theoretical calculations include neo-classical effects. When only Spitzer conductivity is considered the predictions are on average an insignificant few percent higher. The slight systematic differences in fig.11 may be due to $q_0$ being itself a function of $< j > / q_0 j_0$ or to systematic differences between the shapes of the ion and electron pressure and temperature profiles, which at the present we are not able to measure. The theoretical expectations for $< \overline{T}_e > / \hat{T}_e$ are also insensitive on the assumed value of the parameter $\mu$ (in eq. 3.1) and practically indistinguishable for $\mu s < 0.5$.

Fig.12 shows the corresponding measured (diamonds) density profile widths together with those expected (dots) from the theoretical temperature profiles, combined with theoretical pressure profiles using the observed values of the convexity parameter K from

fig.7. There is again a close agreement although the dispersion around the mean value is significantly higher. The existence of peaked density profiles in the absence of an internal particle source implies that there exists an inward drift of particles, such that the ratio of particle diffusivity to drift velocity is equal to the local density scale length. It should be stressed here that experimental density profile widths are independent of the absolute values of density, which vary over one order of magnitude in the dataset and determine the penetration depths of neutrals.

We have fitted the experimental values of $<\overline{p}_e>/\hat{p}_e$, $<\overline{T}_e>/\hat{T}_e$ and $<\overline{n}_e>/\hat{n}_e$ versus $<j>/q_0 j_0$. The fits for latter two are shown in fig.11 and fig.12. The departures of each individual measurement from the mean value is defined for the pressure as

$$\delta(<\overline{p}_e>/\hat{p}_e) = <\overline{p}_e>/\hat{p}_e - \left\langle <\overline{p}_e>/\hat{p}_e \right\rangle_{fit}$$

and likewise for temperature and density. The standard deviations are 0.016 for the pressure and the temperature and 0.044 for the density. Most revealing however are the cross correlations between these deviations, as shown in fig.13. The correlation coefficient between temperature and density profile widths, $C_{tn}$ is a mere 0.14, which is barely significant. For our sample size of 280 a spurious correlation level of 0.06 is expected, disconsidering any correlations introduced by errors in the measurements. Similarly the correlation coefficient of temperature and pressure, $C_{tp}$=0.18, is close to insignificant. This may seem surprising at first since the pressure is calculated as the product of experimental temperature and density. The result is however consistent with our expectation of a stiff temperature profile. On the other hand density and pressure profile widths are clearly correlated with $C_{np}$=0.68, also as expected for a stiff temperature profile.

### *4.4-Discussion*

The above comparison shows that the theory is entirely consistent with the experimental observations over an extraordinarily vast variety of Ohmic L-mode discharges. However from inspection of fig.7 it is clear that these experimental profiles are restricted in shape even further than required by this theory, indicating that is still incomplete. From fig.13 we see that the pressure profiles widths deviate from, what appears to be an average condition, only by 0.016 (typically 2.5-7.5%) which is comparable to the expected experimental errors.

This raises the question whether the discharge is free to adopt any subset of allowable values for the convexity parameter, $0<K<1$, or whether $K$ is itself a prescribed function of $< j > / q_0 j_0$. The fact that the deviation of the electron pressure profile width $\delta(< \overline{p}_e >/ \hat{p}_e)$ is correlated with that of the density, but not that of the temperature, gives us confidence to assert that this small variation corresponds to a true variation in $K$, although the effectively 'visited' interval of $K$ is much smaller than obtained only from the energy principle. From fig.7 we estimate the effectively visited range of K to be typically about 0.2, e.g. the plasma only populates about 20% of its theoretically accessible existence domain.

The reasons for this are likely to reside in physical effects not included in this theory such as transport and possibly MHD stability. We also cannot exclude that an additional fundamental constraint, yet to be uncovered, is at the origin of this restricted range of pressure profile shapes seen in the experiment. The fact that the density profile, of all, exhibits the most variability in the data and is subject to no constraints from this theory suggests that the limited range of K may be a result of particle transport together with the fuelling method used, in this case peripheral fuelling from gas puffing and recycling. This hypothesis may be tested by deep fuelling methods such as pellets, which should lead to more peaked density and pressure profiles while conserving a stiff temperature profile.

There is a candidate explanation why large values of $K$ are not observed for small values of $< j > / q_0 j_0$. Inspection of the theoretical density profiles obtained by applying Ohm's law shows that for every value of $< j > / q_0 j_0$ there is a value of $K$ above which $dn/dx>0$ just outside the $q=1$ surface, corresponding to hollow density profiles. In fig.7 this boundary is indicated as a dashed-dotted line for the case when Spitzer conductivity only is considered in Ohm's law and as a solid line for a typical neo-classical calculation. These lines can be seen to approximate the upper range of the observed values of $K$. A tentative interpretation of the coincidence is that the plasma may lack the physical mechanism which would be necessary to set up an outward particle drift as would be required over a portion of the minor radius in order to create such a hollow density profile. Similarly the lack of low values of $K$ at high $< j > / q_0 j_0$ may reflect the unavoidability of inward drifts. Such inward drifts are predicted to result from neo-classical processes [28,29] and inclusion of particle drifts in a future extension of this theory may lead to a more complete description of profiles in Ohmic tokamak discharges.

Another possible line of theoretical investigation may involve the heat diffusivity. As shown in appendix C, eq.(C.6), the profile of heat diffusivity is related to the convexity

parameter $K$ (fig.15). Hence theoretical predictions (from outside the work presented here) concerning the heat diffusivity profile, would translate into predictions or constraints on $K$. These may lead, through Ohm's law, to conditions on the density profile, thereby establishing a coupling between heat and particle transport.

### *5) Conclusions*

We have investigated the consequences to the Grad-Shafranov equation when the stationary magnetic entropy principle and an energy principle are included as additional constraints for 'clipped' pressure profiles representative of profiles in sawtoothing Ohmic tokamak discharges. This theory predicts a fixed, rigid shape for the toroidal current density for any given values of $q_0$ and the normalised $q=1$ radius, $\lambda$, or alternatively the parameter $< j > B_0 /(j_0 q_0 \hat{B}) \cong < j > /(q_0 j_0)$, which is well defined for shaped discharges. This relation of $\lambda$ and $< j > B_0 /(j_0 q_0 \hat{B})$ is fixed by theory for any given value of $q_0$. In fig.3 the theoretical $q=1$ radii for $q_0 = 0.8$, 0.9 and 1 are plotted versus $< j > /(q_0 j_0)$ together with the inversion radii measured using x-ray tomography for a large number of plasma conditions and shapes, showing good agreement. The theory also predicts, for any value of $\lambda$, a class of pressure profiles parameterised by the positive convexity parameter $K$. For the plasma energy to be at a minimum, $K$ must be less than unity. An example of a current profile and a few examples of pressure profiles are shown in fig.4. In fig.5 the theoretical pressure profiles are compared to experimental electron pressure profiles. 'Clipped' experimental electron pressure profiles, which effectively disregard post crash reheat, are defined for comparison with theory by $\overline{p}_e = \min(p_e, \hat{p}_e)$ where $\hat{p}_e$ is the pressure at the q=1 surface. The widths of these clipped profiles are shown in fig.6 (diamonds) and depend linearly on $< j > /(q_0 j_0)$. The corresponding experimental values of $K$ are for the most part in the theoretical interval $0<K<1$. Instead of populating the whole interval however, the observed values fall into a narrow range, with $K$ increasing from near 0 for $< j > /(q_0 j_0)=0.2$ to near 0.6 for $< j > /(q_0 j_0)=0.6$.

Using Ohm's law for any given current profile, the choice of a particular pressure profile (corresponding to a particular value of $K$) determines the temperature and the density profiles. If Spitzer conductivity alone is considered, the temperature profile is determined by the current profile alone, independently of the pressure profile. Inclusion of neo-classical

effects requires knowledge of the absolute pressures and densities, but is found to have little effect on the shape and the width of the temperature profile, as shown in fig.9. The widths of the 'clipped' electron temperature profiles and density profiles are shown in fig.11 and fig.12a together with the theoretical widths for values of $K$ consistent with the measured widths of the pressure profiles, showing close agreement. As a result of the stiffness of the current profile and Ohm's law, variations in pressure profiles (corresponding to variations in $K$), must be correlated with variations in the density profiles, not however with variations of the temperature profile. This is indeed the case as is seen in fig.13.

The range of variation of the pressure profile is much smaller than the range allowed by the theory as it stands. This may result from the physics governing particle transport and the peripheral fuelling in these discharges. The existence of peaked density profiles in the absence of deep fuelling implies the existence of a particle pinch, the physics of which must itself be sensitive to the parameter $< j > /(q_0 j_0)$. Inclusion of particle transport physics in a future development of this theory may lead to further improvement and possibly a complete predictive description of profile behaviour in Ohmic discharges. Conditions on heat diffusivity, external to the theory presented here, would also constrain $K$ as shown in appendix C.

In summary the experimental evidence supports the prediction of a rigid current profile and an Ohmically relaxed, highly stiff temperature profile. Pressure and especially density profiles are less stiff, although apparently stiffer than expected from the physics included in this theory. Most importantly, this work shows that, contrary to widespread expectance, appropriately formulated statistical concepts can be of relevance to systems driven far from thermodynamical equilibrium, such as tokamak plasmas.

**Acknowledgements.** This work was partly supported by the Swiss National Science Fund. The support of the entire TCV team is gratefully acknowledged.

***References***


[1] Bussac M.N., Pellat R., Edery D. and Soule J.L, *Phys. Rev. Lett.* **35** (1975), 1638

[2] Coppi B., *Comments Plasma Phys. Controlled Fusion* **5** (1980) 261

[3] Biskamp D., *Comments Plasma Phys. Control. Fusion* **10** (1986) 165

[4] Kadomtsev B., Proc. *Int. Conference on Plasma Physics,* Kiev, 6-12.4 (1987) 1273

[5] Taylor J.B. *Phys. Fluids B* **5** (1993) 4378

[6] Arunasalam V. *et al.*, *Nuclear Fusion* **30** (1990) 2111

[7] Weisen H., Behn R., Furno I., Moret J.-M., Sauter O. and the TCV team, *25th EPS on Controlled Fusion and Plasma Physics, Prague,* **ECA 22** (1998) H081PR, 2310, European Physical Society

[8] Weisen H., Behn R., Furno I., Moret J.-M., Sauter O. and the TCV team, *Plasma Physics Contr. Fusion* **40** (1998) 1803

[9] Weisen H., Behn R., Furno I., Moret J.-M., Sauter O. and the TCV team, *Physics of Plasmas* **6** (1999), 1.

[10] Hofmann F., Lister J.B., Anton M. et al., *Plasma Phys. Contr. Fusion* **36** (1994) B277

[11] Minardi E., *J. Plasma Phys.* 48 (1992) 281

[12] Minardi E., *J. Plasma Phys.* 50 (1993) 505

[13] Minardi E., *J. Plasma Phys.***62** part 3 (1999) 319

[14] Garrett, A.J.M. In: *Maximum Entropy in Action* (ed. B Buck and V.A. Macaulay), 1991, p.139. Clarendon Press, Oxford

[15] Gull, S. F. In: *Maximum Entropy in Action* (ed. B Buck and V.A. Macaulay), 1991 p.171. Clarendon Press, Oxford

[16] Jaynes, E.T. 1963 *Information theory and statistical mechanics*. In: *Statistical Physics* 1962, Brandeis Lectures (ed. K.W. Ford) pp.181-218 Benjamin, New York;

[17] Jaynes, E.T. 1983, *Papers on probability, statistics and statistical physics* (ed. R.D. Rosenkrantz) Reidel, Dordrecht

[18] Minardi E., *Plasma Phys. Contr.Fusion* **31** (1989) 229

[19] Taylor, J.B. *Phys. Rev. Lett.* **33**, (1974) 1139

[20] Weisen H., Alberti S., Barry S. *et al.*, *Plasma Physics Contr. Fusion* **39** (1997) B135

[21] Anton M., Weisen H., M.J. Dutch, *Plasma Phys. Control. Fusion* **38** (1996) 1849

[22] Furno I., Weisen H., Moret J.M., Blanchard P. and Anton M., *24th EPS on Controlled Fusion and Plasma Physics* **ECA 21A** part II, 545

[23] Weisen H., Borg G., Joye B., Knight A.J. and Lister J.B., *Phys. Rev. Lett.* **62** (1989) 434

[24] Soltwisch H., *Plasma Physics and Controlled Fusion* **34** (1992) 1669

[25] Levinton F.M., Zakharov L., Batha S.H. *et al.*, *Phys. Rev. Lett* **72** (1994) 2895

[26] Rice, B.W., *Fusion Engineering and Design*, **34-35** (1997) 135

[27] Sauter O, *ITER EDA memo* IdoMS No 19 MD 18 96-08-06 F1 (1996)

[28] Hirshmann S.P., Sigmar D.J., *Nuclear Fusion* **21** (1981) 1079

[29] Kim Y.B., Diamond P.H. and Groebner R.J., *Phys. Fluids* **B** 3 (1991) 2050

# *Figures*

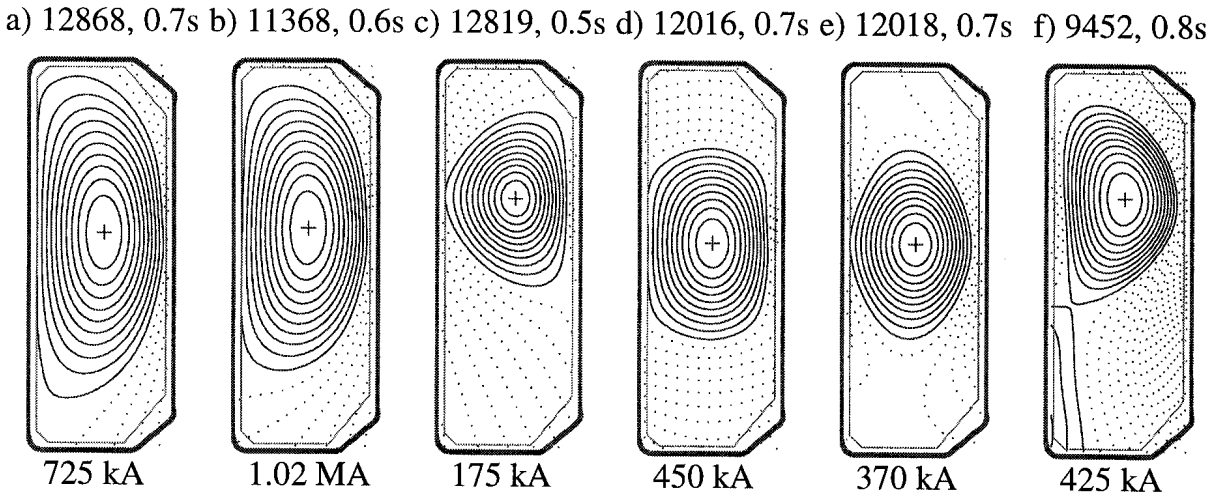


*Fig. 1 Examples of tokamak equilibria in the TCV confinement and profile database.*

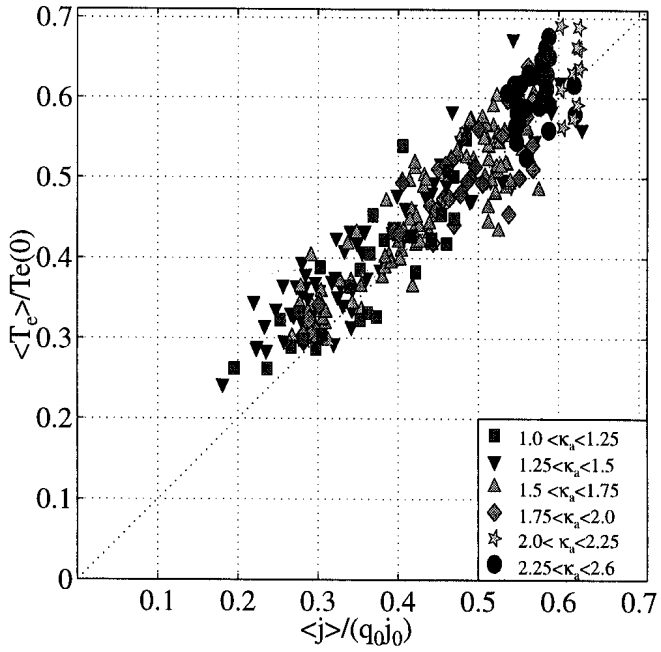


*Fig. 2 Electron temperature profile widths (inverse peaking factors) as function of current profile width parameter. Symbols refer to classes of elongation at the LCFS.*

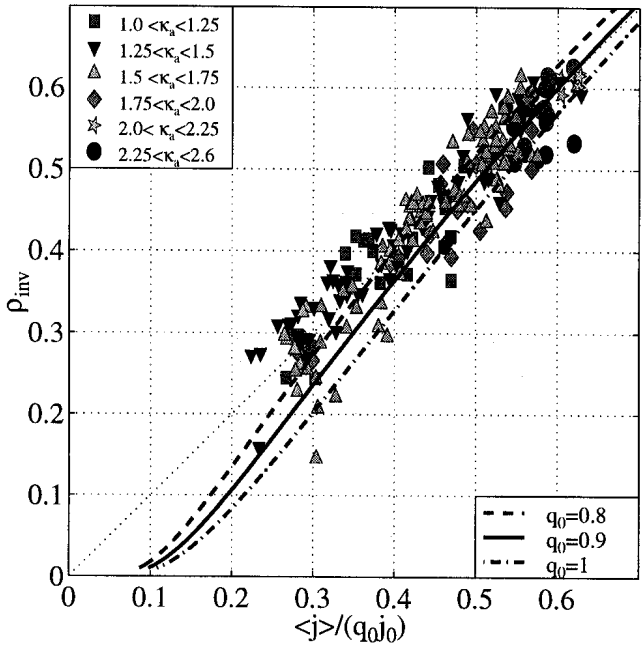


*Fig. 3 Sawtooth inversion radii from x-ray tomography (symbols) and theoretical predictions for q=1 surface (bold lines) for three assumed values of $q_0$.*

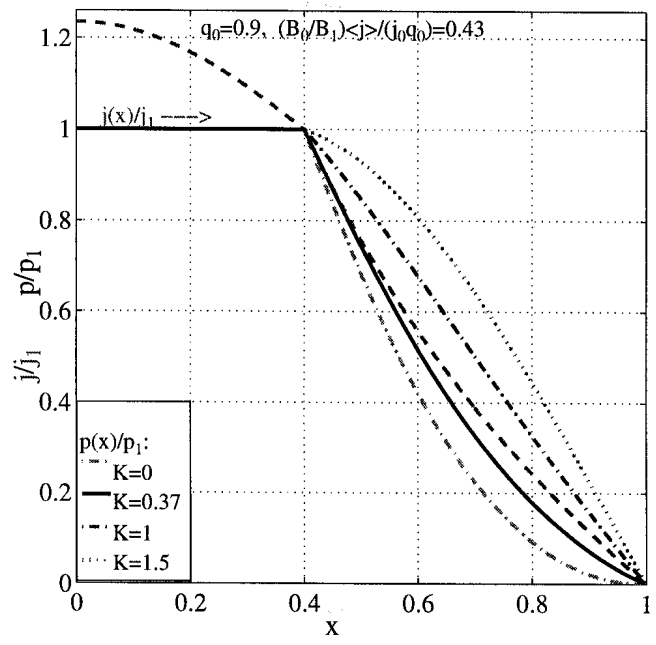


*Fig. 4 Example of current profile (dashed), corresponding to λ=0.4 and four examples of pressure profiles. The continuous line shows a profile as typically observed in the experiment, the dash-dotted lines are theoretically predicted existence boundaries. The dotted profile is "forbidden" according to the energy principle in appendix B.*

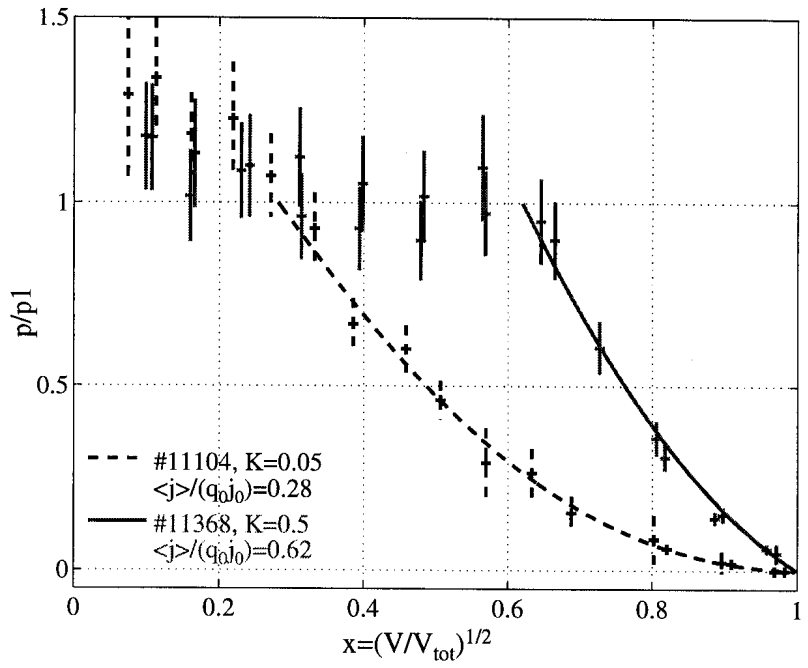


*Fig. 5 Examples of electron pressure profiles in TCV from Thomson scattering and corresponding theoretical profiles outside q=1 surface.*

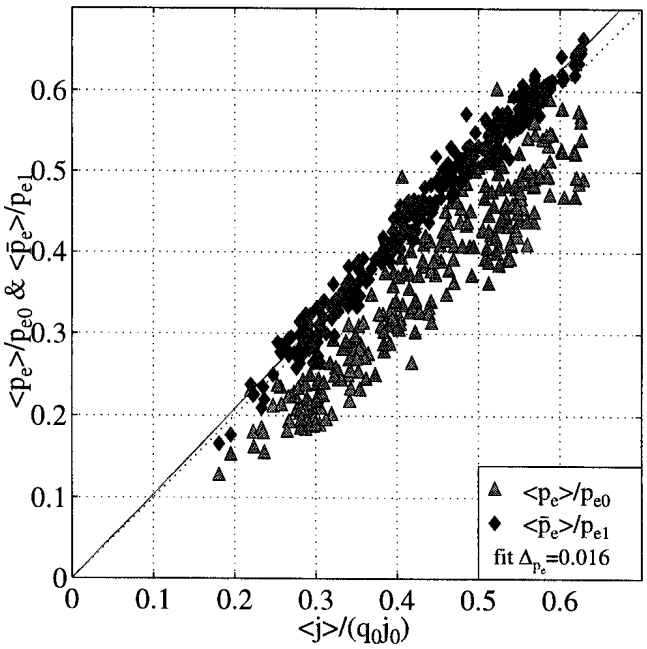


*Fig. 6 Widths of electron pressure profiles (triangles) and clipped electron pressure profiles (diamonds) versus current profile width parameter, assuming $q_0$=0.9. (The slope of the fitted line is 1.04)*

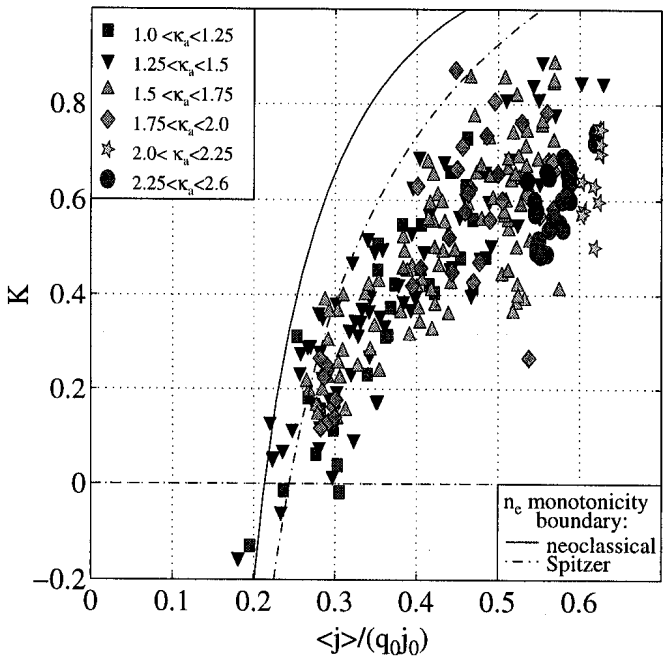


*Fig. 7 Experimental pressure profile convexity parameter K.*

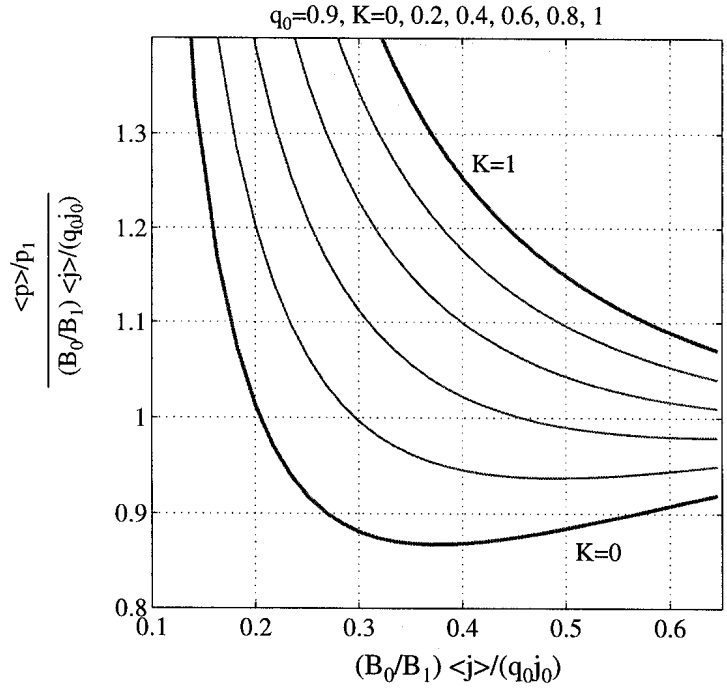


*Fig. 8 Ratio of theoretical pressure and current profile widths factors as function of current profile width factor and several values of the convexity parameter K. Note that the paramagnetic correction* $B_0/B_1$ *is negligibly small.*

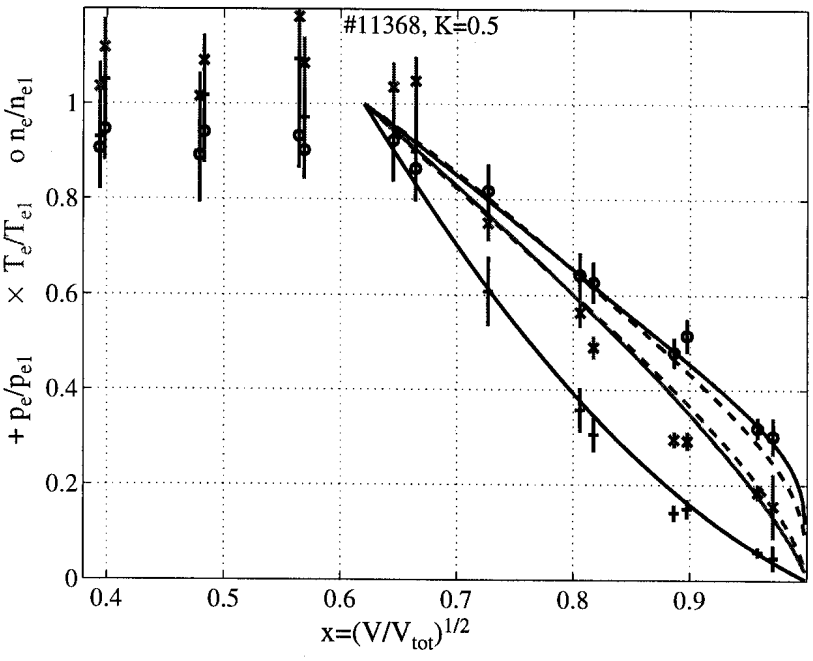


*Fig. 9 Example of experimental electron pressure (+), temperature (x) and density (o) profiles from Thomson scattering, together with theoretical profiles. The continuous lines are obtained using neo-classical Ohm's law, the dashed lines using Spitzer resistivity only.*

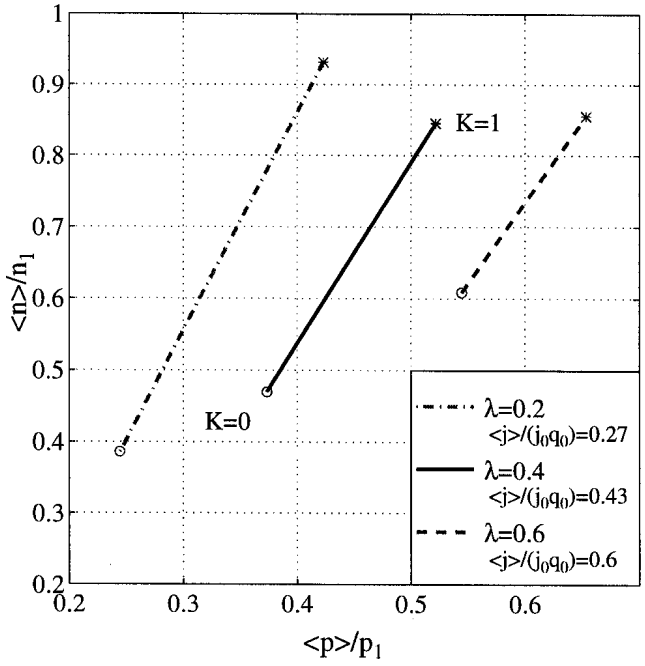


*Fig. 10 Theoretical relation between pressure profile widths and density profile widths.*

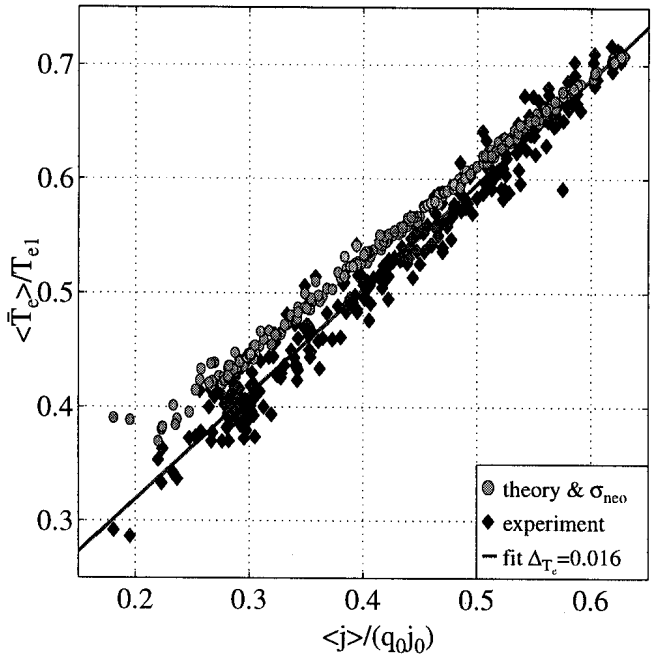


*Fig. 11 Widths of clipped electron temperature profiles. Diamonds: experiment, dots: theory with neo-classical Ohm's law. (Fit: $<\bar{T}_e>/T_{e1}=0.92<j>/(q_0 j_0)+0.13$)*

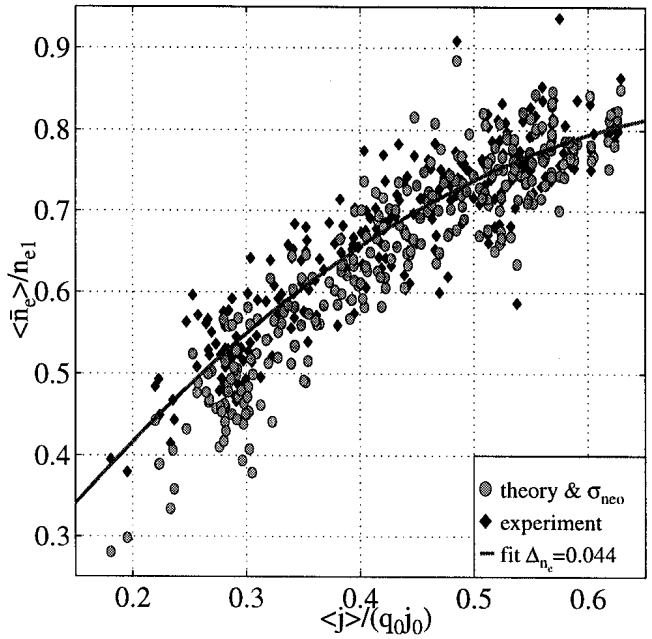


*Fig. 12 Widths of clipped electron density profiles. Diamonds: experiment, dots: theory with neo-classical Ohm's law. (Fit: $<\bar{n}_e>/n_{e1}=-1.27[<j>/(q_0 j_0)]^2+1.95<j>/(q_0 j_0)+0.076$)*

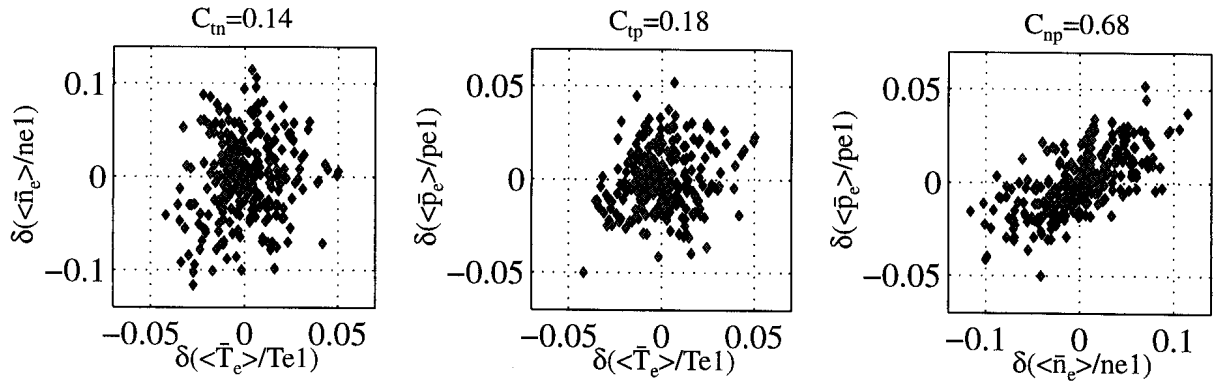


*Fig. 13 Correlation between deviations of electron temperature, density and pressure from mean values.*

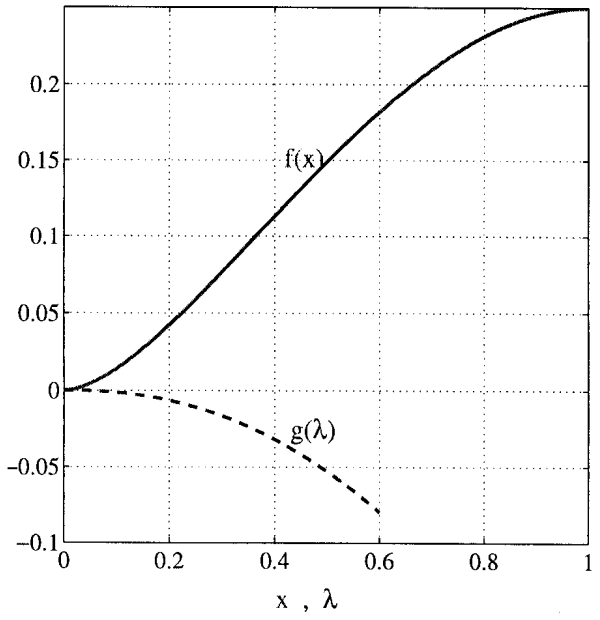


*Fig. 14 Functions g(λ) and f(x) (eq. C7)*

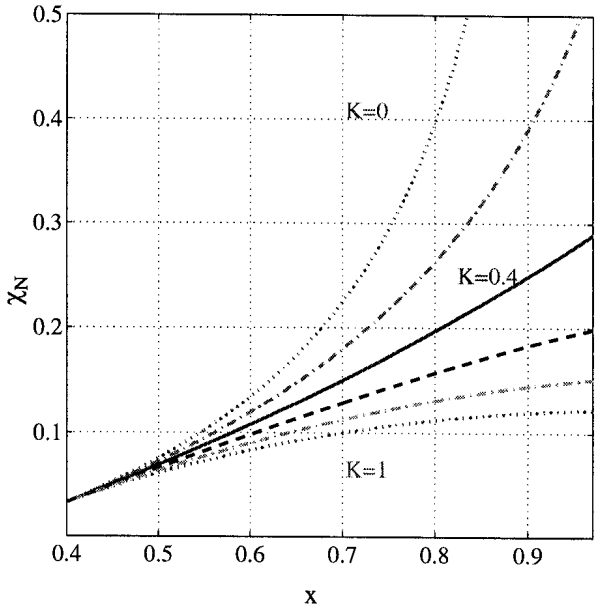


*Fig. 15 Heat diffusivity profiles (eq. C6)*

# Appendixes

## *Appendix A. Determination of the equilibrium profiles*

In this appendix we derive the characteristic profiles of the Ohmic plasma equilibria in a tokamak with constant magnetic entropy.

### *A.1 Compatibility with the Grad-Shafranov-Schlueter equation*

From the Grad-Shafranov-Schlueter equation one has

$$\int_{\Delta\Omega} \vec{E} \bullet \vec{j} dV = E_0 R_0 \int_{\Delta\Omega} \frac{j_\phi}{R} dV = \frac{cE_0 R_0}{4\pi} \int_{\Delta\Omega} \nabla \bullet \frac{\nabla\psi}{R^2} dV = \frac{cE_0 R_0}{4\pi} \int_S \frac{\nabla\psi \bullet d\vec{S}}{R^2} \tag{A.1}$$

Here $\psi$ is the poloidal flux related to $\vec{B}$ by $\vec{B} = B_\phi \vec{e}_\phi + \vec{e}_\phi \times \nabla\psi$, $\vec{j} = \vec{e}_\phi j_\phi$ with $j_\phi$ given by the expression

$$4\pi j_\phi / cR = \nabla \bullet R^{-2} \nabla\psi = -\left[(F^2(\psi))'/2R^2 + 4\pi p'(\psi)\right] \tag{A.2}$$

where $p(\psi)$ is the pressure and $F(\psi) = RB_\phi$ .
Substituting (A.2) and the expression

$$\int_{\Delta\Omega} \vec{E} \bullet \nabla^2 \vec{j} dV = \int_S (E\nabla j_\phi - j_\phi \nabla E) \bullet d\vec{S}, \tag{A.3}$$

in the relation (2.2), the condition $dS / dt = 0$ can be written in terms of surface integrals and is satisfied when the following equality holds

$$\frac{1}{\mu^2} \int_{S_e} (E\nabla j_\phi - j_\phi \nabla E) \bullet d\vec{S} + \frac{cE_0 R_0}{4\pi} \int_{S_e} \frac{\nabla\psi \bullet d\vec{S}}{R^2} = \tag{A.4}$$

$$= \frac{1}{\mu^2} \int_{S_i} (E\nabla j_\phi - j_\phi \nabla E) \bullet d\vec{S} + \frac{cE_0 R_0}{4\pi} \int_{S_i} \frac{\nabla\psi \bullet d\vec{S}}{R^2}$$

where $d\vec{S} = dS\nabla\psi / |\nabla\psi|, S_e, S_i$ are the magnetic surfaces delimiting the internal and the external sides of any toroidal ring situated in the confinement region. It follows that each member of (A.4) must be independent of $\psi$ and equal to a constant $C$. Recalling the expression (A.2) of $j_\phi$ and taking into account the relations

$$\int_S \frac{\vec{e}_R \bullet d\vec{S}}{R} = \int_S \frac{\nabla R \bullet d\vec{S}}{R} = \int_{\Delta\Omega} \nabla^2 (\ln R) dV = 0$$

$$\int_{S(\psi)} \frac{\nabla\psi \bullet d\vec{S}}{R^2} = 2\pi \int_0^{2\pi} \frac{d\psi}{dr}\frac{r}{R} d\theta = 2\pi \int_0^{2\pi} B_\theta r d\theta = \frac{8\pi^2}{c} I(\psi) \qquad \text{(A.5)}$$

where $B_\theta$ is the poloidal field and $I(\psi)$ is the current flowing inside $\psi$, one derives from (A.4) the equality

$$\frac{cp''(\psi)}{\pi I(\psi)} \int_{S(\psi)} \nabla\psi \bullet d\vec{S} + \left(F^2(\psi)\right)' = \qquad \text{(A.6)}$$

$$= 2\mu^2 - \frac{C}{\pi E_0 R_0 I(\psi)}$$

which is a condition on the functions $p(\psi)$ and $F(\psi)$. Thus, introducing an arbitrary function $\varepsilon(\psi)$, one splits this relation in two independent equations for $p(\psi)$ and $F(\psi)$

$$p''(\psi) \int_{S(\psi)} \nabla\psi \bullet d\vec{S} = -\frac{\varepsilon(\psi) C}{cE_0 R_0} \qquad \text{(A.7a)}$$

$$(F^2(\psi))'' = 2\mu^2 - (1 - \varepsilon(\psi))\frac{C}{\pi E_0 R_0 I(\psi)} \qquad \text{(A.7b)}$$

In this way the introduction of the condition of stationary entropy reduces the indeterminacy of the toroidal equilibrium due to the two arbitrary functions $p(\psi)$ and $F(\psi)$ to that of the single function $\varepsilon(\psi)$. Further, we shall see that $\varepsilon$ must be a constant as a consequence of the validity of a minimum principle for the plasma energy (see Appendix B).

We now proceed assuming for simplicity the cylindrical approximation. A first integration of the eqs.(A.7a & b) gives

$$p'(\psi) = A - \frac{\varepsilon C}{4\pi^2 c R_0^2 E_0} \ln\frac{r}{s} \qquad \text{(A.8a)}$$

$$\left(F^2(\psi)\right)' = 2\mu^2\psi - (1-\varepsilon)\frac{2C}{\pi c E_0} \ln\frac{r}{s} + 2C_0 \qquad \text{(A.8b)}$$

where $A$ and $C_0$ are constants. Taking into account these relations in (A.2) the expression for $j_\phi$ becomes

$$j_\phi = -\frac{c}{4\pi}\left\{\frac{\mu^2\psi}{R_0} + \frac{C_0}{R_0} + 4\pi R_0 A - \frac{C}{\pi c E_0 R_0} \ln\frac{r}{s}\right\} \qquad \text{(A.9)}$$

Applying the $\nabla^2$-operator to this equation and recalling the D'Alembert law

$$\nabla^2\psi = \frac{4\pi R_0}{c} j_\phi \tag{A.10}$$

one sees that $j_\phi$ must satisfy the equation

$$\nabla^2 j_\phi + \mu^2 j_\phi = 0 \tag{A.11}$$

The two equations (A.10) and (A.11) above and the boundary conditions determine completely the poloidal configuration of the magnetic field. Once the poloidal flux $\psi$ is known, the pressure and the toroidal field follow from integration of the eqs.(A.8a & b).

### *A.2 The poloidal configuration*

The poloidal magnetic configuration in the confinement region, $s\lambda \le r \le s$, is determined by eq.(3.1) of the text. Inside the surface $\hat{q} = 1$ a safety factor profile of the form $q = q_0 + (1 - q_0) r^2 / (s\lambda)^2$ is assumed, according to a model already applied to the discussion of the TCV data [7-9], where $q_0$, $j_0$ and $B_0$ are the axial values of $q$, $j$ and $B$ with $q_0 = cB_0 / 2\pi R_0 j_o$. The relation $\hat{j} = j_0 q_0^2 \hat{B} / B_0$ then holds on the $\hat{q} = 1$ surface.

Putting in eq.(A.9) $\psi = 0$ at $r = s$, one has $C_0 = -4\pi R_0^2 A$ and one obtains the following expression for the poloidal flux in the confinement zone

$$\psi = \frac{4\pi R_0}{c\mu^2}\left( -j + \frac{C}{4\pi^2 R_0 E_0} \ln\frac{r}{s} \right) \tag{A.12}$$

The constant $C$ is fixed by continuity of the poloidal field $B_\theta = (1/R) d\psi / dr$ across the surface $\hat{q} = 1$ where $\hat{B}_\theta = 2\hat{I} / cs\lambda = s\lambda \hat{B} / R_0$, $\hat{I} = j_0 q_0 \pi (s\lambda)^2 \hat{B} / B_0$ being the current flowing in the sawteeth zone. One finds

$$\frac{C q_0}{4\pi^2 E_0 R_0 \hat{j}} = \frac{(\lambda\mu s)^2}{2}\left( 1 - \frac{2\Lambda q_0}{D\lambda\mu s} \right) \equiv \beta \tag{A.13}$$

where $\Lambda$ is given by eq.(3.4).

Finally, eq.(3.1) determines the following relation between the safety factor at the edge, $q_s = sB_{ext} / R_0 B_\theta(s)$, and the position $\lambda$ of the $\hat{q} = 1$ surface

$$\frac{1}{q_s}\frac{B_{ext}}{\hat{B}} = \lambda^2 - \frac{2q_0}{\mu s D}\left(\frac{2}{\pi\mu s} + \lambda\Lambda\right) \tag{A.14}$$

The left hand side of this equality can be expressed in terms of the average current density $< j >= I(s)/\pi s^2$ applying the relation $(1/q_s)(B_{ext}/\hat{B}) = < j > B_0 / j_0 q_o \hat{B}$ which follows from the definitions introduced above. Then one obtains the equation (3.3) of the text.

### *A.3 The plasma pressure profile*

The integration of eq.(A.8a) with the condition $\psi = 0$ at $r = s$ leads to the equality

$$p(\psi) = A\psi - \frac{\varepsilon\beta \cdot \hat{j}}{cR_0 q_0}\int_0^{\psi} d\psi \ln x \tag{A.15}$$

where $A$ is determined by imposing $p(\hat{\psi}) = \hat{p}$ on the surface $\hat{q} = 1$. Recalling the definitions (3.6) the normalized expression for $p$ becomes

$$\frac{p(\Psi)}{\hat{p}} = \frac{\Psi}{\hat{\Psi}} + \varepsilon\frac{\hat{B}^2\beta}{\pi R_0^2 \mu^2 \hat{p}} Y(\Psi) \tag{A.16}$$

It is now convenient to express the parameter $\varepsilon$ in terms of the average pressure $< p >$. Let us denote with $\overline{Q}$ the average of $Q$ in the confinement region

$$\overline{Q} = \frac{2}{1-\lambda^2}\int_{\lambda}^{1} Qx dx \tag{A.17}$$

Taking $p$ as uniform in the sawteeth zone and equal to $\hat{p}$, one has the following relation

$$\frac{< p >}{\hat{p}} = \lambda^2 + \frac{\overline{p}}{\hat{p}}(1-\lambda^2) \tag{A.18}$$

Thus, the $\overline{p}$ -average of (A.16) determines $\varepsilon$ in terms of $< p >$ and $p(x)$ takes the following form

$$\frac{p(x)}{\hat{p}} = \frac{\Psi(x)}{\hat{\Psi}} + \frac{Y(x)}{\overline{Y}}\left(\frac{1}{1-\lambda^2}\left(\frac{< p >}{\hat{p}} - \lambda^2\right) - \frac{\overline{\Psi}}{\hat{\Psi}}\right) \tag{A.19}$$

that shows that the pressure profile is characterized only by $< p > / \hat{p}$ and by the poloidal magnetic configuration which is fixed by $\lambda$ (or $< j > B_0 / j_0 q_0 \hat{B}$). The parameterization of $p$ can be further simplified introducing a convenient parameter $K$, defined by the expression

$$K\left(< j > B_0 / j_0 q_0 \hat{B}, < p > / \hat{p}\right) \equiv 1 + \frac{\hat{X}}{\overline{\Psi}}\left(\frac{1}{1-\lambda^2}\left(\frac{< p >}{\hat{p}} - \lambda^2\right) - \frac{\overline{\Psi}}{\hat{\Psi}}\right) \qquad \text{(A.20)}$$

Introducing this expression into (A.19) one obtains the equation (3.5) of the main text.

### *A.4 The toroidal field*

The elimination of the logarithmic term between the eqs.(A.8 a & b) leads to the equality

$$\left(F^2(\psi)\right)' = 2\mu^2\psi + \frac{8\pi R_0^2}{\varepsilon}\left(p'(\psi) - A\right) - 8\pi R_0^2 p'(\psi) \qquad \text{(A.21)}$$

The integration between $\psi$ and $\psi = 0$ gives

$$R_0^2\left(B_{ext}^2 - B^2\right) = -\mu^2\psi^2 - \frac{8\pi R_0^2}{\varepsilon}\left(p - A\psi\right) + 8\pi R_0^2 p \qquad \text{(A.22)}$$

Finally, applying (A.15) one obtains in leading approximation ( $\hat{B} / B_{ext} \approx 1$),

$$\left(\frac{B}{B_{ext}}\right)^2 = 1 + \frac{4\Psi^2}{(R_0\mu)^2} - \frac{8\beta X}{(R_0\mu)^2} - \frac{8\pi p}{B_{ext}^2} \qquad \text{(A.23)}$$

where $B_{ext} = F(0)R_0$.

This relation shows that $\hat{B} / B_{ext}$ is independent of $\varepsilon$ and is entirely determined by $\lambda$ or $< j > /(j_0 q_0)$ and by $\hat{p} / B_{ext}^2$.

## *Appendix B. Minimum principle for plasma energy*

As we have seen in A.3, the pressure profile, eq. (A.15), follows from the requirement that the Grad-Shafranov-Schlueter equilibria satisfy the condition of constant magnetic entropy. It will be shown here that the same profile follows by minimising the plasma energy of a tokamak state with constant magnetic entropy and constant total current. At the same time the function $\varepsilon(\psi)$, which is not determined by the compatibility requirement above, is shown to be a constant such that $K > 1$ , consistently with the minimisation procedure and in agreement with what has been assumed in (3.18) and in the experimental comparisons.

The magnetic entropy of a generic stationary magnetic configuration is given by eq.(2.1) (apart from a positive coefficient)

$$S \propto -\int \vec{j}^{\,2} dV + \frac{\mu^2 c}{4\pi} \int \vec{j} \bullet \vec{A} dV \tag{B.1}$$

In the case of a tokamak state with constant entropy, $\vec{j} = \vec{e}_\varphi j$ is the toroidal current density given by (A.11). Applying (A.10) one can see that $j$ can be expressed always as the sum of a linear function of $\psi$ and of a harmonic function of $r$. Specifically, recalling (A.13) and (A.14) we have

$$j = -\frac{c\mu^2}{4\pi R_0}\psi + \frac{\hat{\beta j}}{q_0} \ln \frac{r}{s} \tag{B.2}$$

where $\psi = -RA_\phi$. We minimise the plasma energy $U = (3/2)\int p dV$ with respect to arbitrary variations $\delta\psi$ of $\psi$ in the confinement zone under constant entropy $S$ and constant total current $I = 2\pi \int jrdr$. The variational procedure involves the vanishing of the following first variation

$$\delta(U + \eta_1 S + \eta_2 I) = 0 \tag{B.3}$$

where $\eta_1$ and $\eta_2$ are Lagrange multipliers (the coefficient of $S$ is absorbed into $\eta_1$ ). Noting that $\delta j = -(c\mu^2 / 4\pi R_0)\delta\psi$ in accordance with (B.2), the first variation (B.3) takes the form

$$\int dV \left( \frac{3}{2} p'(\psi)\delta\psi - \eta_1 \left( 2j\delta j + \frac{\mu^2 c}{4\pi R_0}(\psi \delta j + j\delta\psi) \right) + \frac{\eta_2}{2\pi R_0}\delta\psi \right) =$$

$$= \int dV \left( \frac{3}{2} p'(\psi) + \eta_1 \frac{\mu^2 c}{2\pi R_0} \frac{\hat{\beta j}}{q_0} \ln\left(\frac{r}{s}\right) - \eta_2 \frac{\mu^2 c}{8\pi^2 R_0^2} \right) \delta\psi = 0 \tag{B.4}$$

The integrand must vanish in view of the arbitrariness of $\delta\psi$ and one obtains

$$p'(\psi) = \eta_2 \frac{\mu^2 c}{12\pi^2 R_0^2} - \eta_1 \frac{\mu c^2}{3\pi R_0} \frac{\hat{\beta j}}{q_0} \ln \frac{r}{s} \tag{B.5}$$

This expression has just the same form as that given by (A.8a) where $A$, as well as $\varepsilon$, are constants and are replaced in (B.5) by the Lagrange multipliers $\eta_1$ and $\eta_2$. These multipliers

are fixed in order to satisfy the same conditions that lead, after integration, to the expressions (A.15) or (A.20) for $p(\psi)$.

It remains to be shown that $U$ is indeed a minimum. Considering the second variation of $U$

$$\delta^2 U = \frac{3}{2}\int p''(\psi)\frac{(\delta\psi)^2}{2}dV = \frac{3}{16}(1-K)\frac{c\hat{p}\mu^2}{\hat{B}R_0\hat{X}}\int\frac{(\delta\psi)^2}{I(r)}dV \tag{B.6}$$

one sees that when $K<1$ , $\delta^2 U$ is positive and therefore $U$ is minimum. Consistently with the derivation above, the minimum of $U$ is relaxed when the magnetic entropy is not constant, for instance when a neighbouring equilibrium exists to which the system evolves by increasing the entropy, as is the case of the L-H transition [13]. In that case the plasma energy is indeed seen to increase.

### *Appendix C. Conditions on effective thermal diffusivity*

The consistency with the power balance equation of the constant entropy, pressure and temperature profiles implies stringent conditions on the heat flux and on the effective thermal diffusivity, as will be discussed presently. Recalling (2.2) and (A.3) the condition $dS/dt = 0$ of stationary magnetic entropy takes the form

$$-\frac{1}{\mu^2}\int_S (E\nabla j - j\nabla E)\bullet d\vec{S} = \int \vec{E}\bullet\vec{j}dV \tag{C.1}$$

Comparing this with the equation for the power balance in a stationary plasma (in the one-fluid approximation)

$$\int_S \vec{q}_h \bullet d\vec{S} = \int_V \vec{E}\bullet\vec{j}dV \tag{C.2}$$

one finds the following relation for the heat flux in the confinement zone

$$\int_S \vec{q}_h \bullet d\vec{S} = -\frac{1}{\mu^2}\int_S (E\nabla j - j\nabla E)\bullet d\vec{S} \tag{C.3}$$

An effective thermal diffusivity $\chi_{eff} = -q_h / n\nabla T$ can then be defined which is related to the poloidal magnetic configuration according to the following relations (in cylindrical approximation)

$$\chi_{eff} = \frac{E_0}{\mu^2 n\nabla T}\left(\frac{dj}{dr} - \frac{\hat{j}\beta}{q_0 r}\right) = -\frac{cE_0}{4\pi R_0 n\nabla T}\frac{d\psi}{dr} = -\frac{cE_0}{4\pi n\nabla T}B_\theta(r) \qquad \text{(C.4)}$$

where (A.13) and (3.14) have been used. The term involving $\beta$ would describe a divergenceless contribution to $\vec{q}_h$, but this is cancelled by a similar contribution contained in $dj/dr$, as will be shown below. One sees that the continuity of $B_\theta$ implies automatically the continuity of the heat flux everywhere.

In the case of Ohmic relaxation, $j = E_0 T^{3/2} / A(Z_{eff})$ (where $A(Z_{eff})$ is related to the Spitzer resistivity and $Z_{eff}$ is taken as uniform) one can write

$$\chi_{eff} = \frac{3E_0 \hat{j} s^2}{2\hat{p}}\chi_N(r) \qquad \text{(C.5)}$$

where $\chi_N$ is a profile function with the form

$$\chi_N = \frac{j(r)/\hat{j}}{(\mu s)^2 p(r)/\hat{p}}\left(1 - \frac{\beta\hat{j}}{q_0 r dj/dr}\right) \qquad \text{(C.6)}$$

For small $\mu s$ the term in brackets can be split in two functions of $\lambda$ and $x$ respectively

$$\frac{1}{(\mu s)^2}\left(1 - \frac{\beta\hat{j}}{q_0 r dj/dr}\right) = g(\lambda) + f(x) + 0\left((\mu s)^2\right) \qquad \text{(C.7)}$$

The functions $g(\lambda)$ and $f(x)$ are plotted in fig.14. The profile function $\chi_N(x)$ is plotted in fig.15 for $\lambda = 0.4$ and for $K$ in the range $0 < K < 1$ which corresponds to the minimum of the plasma energy and to the concavity of the pressure profiles. As seen in the figure, the minimum principle implies that the thermal diffusivity increases with the minor radius.